Robotic Radiosurgery with Beams of Adaptable Shapes

Achim Schweikard[1,2], Rhea Tombropoulos[1], John R. Adler[2]

[1] Robotics Laboratory, Department of Computer Science
[2] Department of Neurosurgery
Stanford University, Stanford, CA 94305, USA, as@cs.stanford.edu

Abstract: *In radiosurgery, a moving beam of radiation acts as an ablative surgical instrument. Conventional systems for radiosurgery use a cylindrical radiation beam of fixed cross-section. The radiation source can only be moved along simple standardized paths. A new radiosurgical system based on a six degree-of-freedom robotic arm has been developed to overcome limitations of conventional systems. We address the following question: Can dose distributions generated by robotic radiosurgery be improved by using non-cylindrical radiation beams of adaptable cross-section? Geometric methods for planning the shape of the beam in addition to planning beam motion are developed. Design criteria considered in this context are: treatment time, radiation penumbra as well as transparency of interactive treatment planning. An experimental evaluation compares distributions generated with our new radiosurgical system using cylindrical beams to distributions generated with beams of adaptable shapes.*

1 Introduction

In radiosurgery, a radiation beam generated by a moving linear accelerator is used to destroy brain tumors. By combining cross-firing from multiple directions with precision targeting, the radiation beam acts as an ablative surgical instrument.

A *collimator*, typically made of heavy metal is used for focusing and shaping the radiation beam. Conventional radiosurgical systems use static collimators producing cylindrical beams [5, 6, 8]. Cylindrical beams yield adequate distributions for spherical tumors. Our previous research has demonstrated that non-spherical dose distributions can be produced by moving a cylinder beam along appropriate paths. However, collimators of non-cylindrical shape are most natural for producing non-spherical dose distributions. In addition to a substantial improvement in distribution characteristics, non-cylindrical collimators allow for reduction of treatment time. The goal of this research is the design of a collimator and corresponding planning methods suiting the requirements of robotic radiosurgery. Two types of mechanical collimator designs can be used to produce beams of adaptable shapes:

- multi-leaf collimator (fig. 1-a)
- jaw collimator (fig. 1-b)

A jaw collimator produces a beam of rectangular cross-section. Fig. 1-c shows how non-rectangular beams with given planar cross-section can be pro-

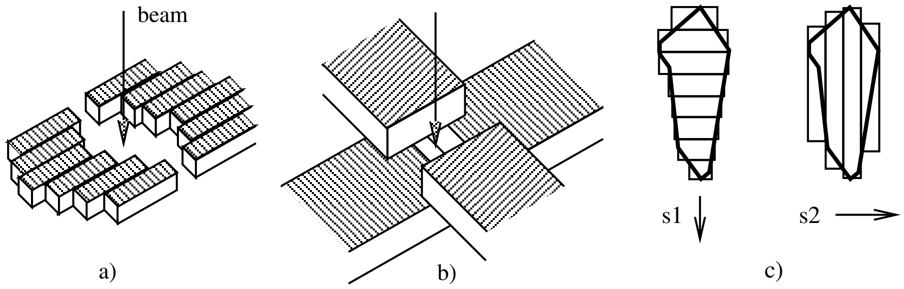

Fig. 1. a) Multi-leaf collimator: rectangular fingers can be moved under computer control. b) Jaw collimator. Jaws can be moved under computer control. Beam cross-section is rectangular. c) To produce a beam of given polygonal cross-section with a jaw collimator, the polygon is covered by a series of parallel rectangles. $s1$, $s2$ are called sweeping directions. Radiation time/number of rectangles depends on sweeping direction.

duced with a jaw collimator: A series of rectangular beams with varying size is overlaid.

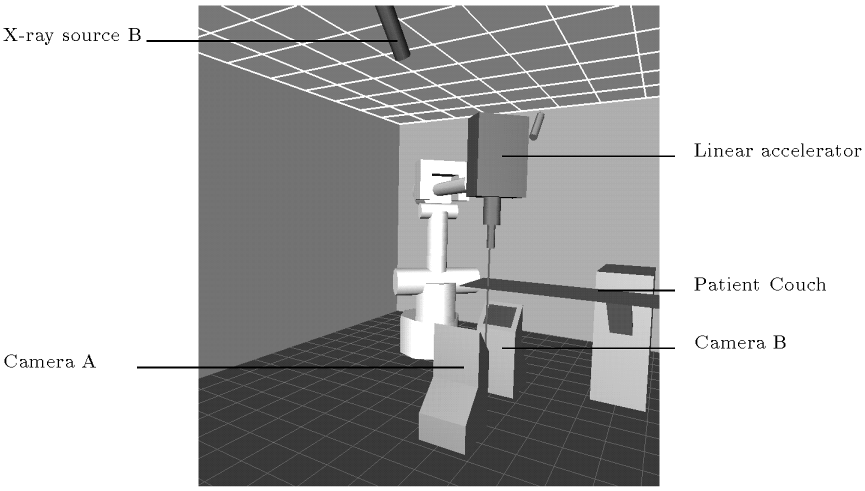

Fig. 2. N-1000 radiosurgical system; robot workspace

1.1 Previous Work

In an interdisciplinary project between the Departments of Neurosurgery and the Department of Computer Science at Stanford University, geometric treatment planning methods for conventional systems were developed [9]. This project led to the design of treatment procedures for image-guided radiosurgery with the

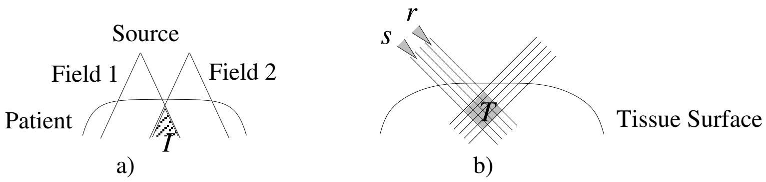

Fig. 3. a)Aligning two separate large radiation fields results in undesirable dose inhomogeneity; the intersection region I will receive high dose, since the radiation source is a point. b)To achieve homogeneity within region T, weight of beam r should be smaller than weight of s, since dose is reduced with depth in tissue.

Neurotron-1000 system in cooperation with Accuray, Inc., Santa Clara [10]. The Neurotron-1000 (N-1000) is a new radiosurgical system with the following features (fig. 2).

- The mechanical gantry is a GM-Fanuc robotic arm with 6 degrees of freedom, which allows for arbitrary spatial paths of the radiation beam. In contrast, conventional systems can only perform simple standardized motions.

- An on-line vision system (with two orthogonal X-ray cameras) determines the position of the patient's skull once a second. In this way, patient motion can be tracked.

- A treatment planning system (*inverse dosimetry*) computes beam paths for generating a dose distribution satisfying specifications input by the surgeon (homogeneous and focussed dose in the tumor, reduced doses in healthy tissues).

The on-line vision system removes the need for the painful stereotaxic frame. Consequently the vision system allows for fractionated treatment. To date, three patients have been treated with a prototype of the N-1000 system at Stanford University Medical Center. Given the flexibility of the new system, it is expected that radiosurgical procedures will replace conventional radiation methods as well as conventional surgery in many instances.

1.2 Related Research

Nedzi, Kooy et al. [7] investigate characteristics of so-called single beam field-shaping paradigms. In particular, their analysis and simulations suggest that an ideal multi-leaf collimator has significant advantages over collimation methods currently in clinical use. They also give design recommendations for an actual implementation of collimators suitable for radiosurgery. Carol [1] describes an implementation of a multi-leaf collimator for a conventional radiosurgical system. The methods in [1, 7] use a single beam for each planar field. In contrast, the approach illustrated in fig. 1-c uses a series of beams for each (planar) field. This paradigm has two advantages over single-beam field shaping, including ideal multi-leaf collimation.

- General beam shapes can be produced. In particular, the beam cross-section does not have to be monotonic. The example in fig. 3-a shows that it is generally not practical to cover fields by aligning two or more large subfields.

• The hardware required for a jaw collimator is comparatively simple and inexpensive. This reduces the cost of required safety features.

• The radiation penumbra can be controlled by using rectangles of varying widths.

• The beams for individual rectangular fields can be *weighted*, i.e. predetermined dose can be assigned to each rectangle. In this way, we can take into account the decrease of dose with depth in tissue (fig. 3-b). In addition, a very simple geometric method for generating non-convex regions of high dose is obtained. The derived algorithms are resolution-complete, i.e. at an appropriate resolution, it can be guaranteed that beam weights generating a distribution specified by the user will be found, if such a distribution can exist. In this way we can avoid problems arising with standard optimization techniques.

Experiments suggest that multiple-beam methods allow for improved dose distributions when compared to conventional collimation methods. However, the use of adaptable collimators must be supported by computer-based planning methods. The planning methods described below are based on an analysis of trade-offs between total radiation time and penumbra, methods for appropriate partitoning of planar fields as well as geometric algorithms for beam weighting.

2 Planning paradigms

We consider a jaw collimator (fig. 1-b). Two pairs of jaws, orthogonal to each other, produce a rectangular beam. The length and width of the (rectangular) beam cross-section can be changed during treatment. Instead of aligning rectangles as in fig. 1-c, we *overlay* a larger number of (parallel) rectangles with small displacement. The direction of displacement is called *sweeping direction*. This avoids problems stemming from alignment inaccuracy and yields higher dose homogeneity. Note that the collimator jaws never move during beam activation. Collimator motion during activation would require additional safety features and accurate velocity control. Our experiments for the N-1000 system show that sufficient homogeneity can be achieved with a small number of rectangles if many beam directions are used.

Fig. 4 illustrates improvements in beam characteristics achievable by combining the kinematic flexibility of a six degree-of-freedom robotic arm with adaptable collimation. Given full kinematic flexibility, the beam can translate along any given direction. Thus the motion along the sweeping direction can be performed by the radiation source (fig. 4-b). Both penumbra and conicity angle can be reduced.

2.1 Reduction of Radiation Time

The output dose rate of commercial linear accelerators is limited. The time required to deliver a fixed dose to every point within a planar field does not

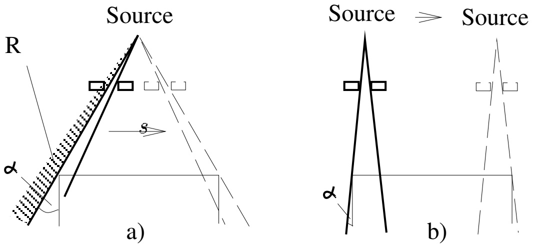

Fig. 4. a) sweeping motion (in direction s) is performed by collimator jaws; b) sweeping motion is performed by radiation source. Beam conicity angle α is reduced in case b). In addition, the size of the penumbral region R can be reduced in case b).

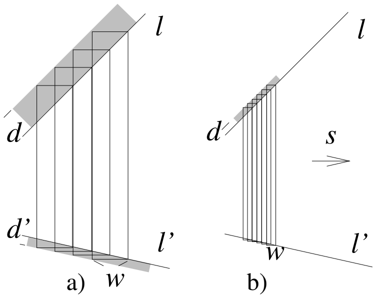

Fig. 5. Radiation penumbra is influenced by slope of polygon edges as well as rectangle width; a) Field edges l, l', widths d, d' of penumbral region, rectangle width w. Slope of edge l with respect to sweeping direction s is higher than slope of edge l'. Therefore penumbral region at edge l is wider than at edge l'. b) Reducing rectangle width w reduces width d of penumbral region.

increase with the field size. Thus, irradiating a given planar field with a series of 50 "pencil beams" of small cross-section instead of one single beam will lead to a (well over) 50-fold increase in required radiation time. Consider the example in fig. 1-c. The number of rectangles needed to cover the given polygon (at a fixed density) depends on the sweeping direction s. Direction $s2$ in fig. 1-c requires less rectangles than direction $s1$.

Large penumbra in the tissue surrounding a tumor is undesirable, and should be reduced as much as possible. Fig. 5 illustrates the trade-offs between total radiation time and penumbra. Increasing the (rectangle) width of each beam will lead to shorter radiation time but increased penumbra.

Our planning method proceeds as follows. A polyhedral reconstruction of the tumor shape is computed from the input data. This reconstruction is projected onto a series of planes through the origin. The normal vectors of these planes are chosen from a large regular grid of points on the 3D unit sphere. In each projection, we obtain a polygonal *field*.

Consider a sweeping direction s in the plane. Assume s is the horizontal direction. We divide the given polygonal field into a series of trapezoidal slabs, obtained by drawing vertical partitioning lines through all polygon vertices. Note that the decomposition into trapezoids changes as the sweeping direction s varies.

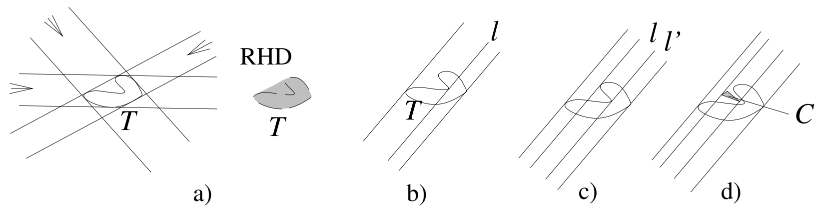

Fig. 6. a)If T is irradiated from multiple directions, such that each field is covered homogeneously, then the region of high dose is convex, and may cover a critical region surrounded by the tumor. b)-d) Partitioning fields; b) Convex-Hull subtraction. Lines passing through $Conv(T) \setminus T$ are separated from remaining lines. c) Monotonic subregions. Lines crossing boundary of T more than twice are separated from other lines. d) Partitoning induced by user defined critical regions.

For the fixed direction s, the penumbra along the upper and lower edge of a single slab is proportional to the rectangle width w.

For each (planar) field, the planning system computes a sweeping direction and a set of rectangle widths for each slab, such that the field is covered with the minimum number of rectangles. Values for the required homogeneity (density of rectangles) as well as maximum allowable (planar) penumbra are entered by the user. The rectangle width of the output path can change between trapezoids, but not within one trapezoid. The functional dependency of edge slope and penumbra is approximated by a series of linear equations with values taken from measurements.

Our current implementation computes the sweeping direction by discretizing, i.e. by considering a series of fixed orientations, and computing the number of polygons required at each such orientation. In this way, we obtain a path minimizing total radiation time, given user-defined homogeneity and penumbra values.

2.2 Non-convex Fields

By region of high dose (RHD) we denote the region (in 3-D space) receiving 80% or more of the maximum dose. As described above, we irradiate a tumor from a set of directions, given as a grid of vectors on the unit sphere. For each direction d the projection of the tumor along d is a (planar) polygon.

For many larger extra-cranial lesions, the tumor is non-convex, and there are critical healthy regions surrounded by the tumor. Such regions should not be part of the RHD, but will be covered by the RHD if we irradiate all fields homogeneously (fig. 6-a). This is undesirable in many cases. An example are tumors of the spine, growing around the spinal cord.

In addition, some of the directions thus chosen may pass through critical healthy structures. Such directions should receive lower *dose weight*.

To address the two problems mentioned, we compute distinct weights for the rectangular beams to be overlaid. Planar fields are partitioned into subregions. Each subregion can then be irradiated with an individual weight. There are several possibilities for partitioning fields. Fig. 6-b,c shows two examples. In case b), a field partitioning is obtained by considering the convex hull of T. T is subtracted from its convex hull, i.e. we set $S = Conv(T) \setminus T$. Beams (lines) passing through S are separated from the remaining beams (lines). The partitioning of each planar field induced by this separation can be computed automatically, and a distinct weight can be assigned to each sub-field thus obtained.

Case c) shows a different way to obtain a field partitioning. We call a line *monotonic* with respect to T if it crosses the boundary of T at most twice. Thus, in fig. 6-c, lines above l and lines below l' are monotonic with respect to T. Lines between l and l' are non-monotonic. To obtain a field partitioning using monotonicity we can separate monotonic beams (beams crossing the tumor boundary at most twice) from non-monotonic beams. The example shows that methods a) and b) will yield distinct partitionings in general. We thus do not fully automatize field partitioning. Instead, we use a semi-manual method (fig. 6-d). This method allows for improved user-control. The user delineates a structure C on the tomographic images. Given this (two-dimensional) delineation, we compute a three-dimensional reconstruction of C by thickening between tomographic cross-planes. Each field is then split into two sets; lines passing through C are separated from the remaining lines. After this, we compute the *arrangement* of beams thus obtained and apply the weighting method in [10] to assign weights to each (rectangular) beam. The user can change the delineation of C interactively to obtain distinct partitionings.

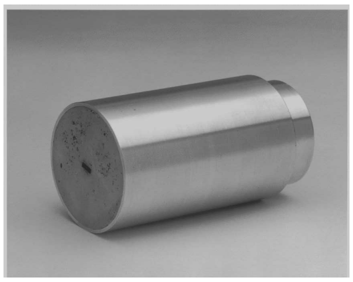

Fig. 7. Collimator for N-1000 system; conic beam with rectangular cross-section.

3 Experiments

The described methods were implemented in the context of the Neurotron-1000 system. While the characteristics of larger rectangular beams are comparatively well-known, it is difficult of provide adequate simulations for small rectangular fields. To verify characteristics of very small rectangular beams with the N-1000 system, a collimator with static rectangular cross-section (5 mm by 15 mm cross-section at target) was manufactured (fig. 7).

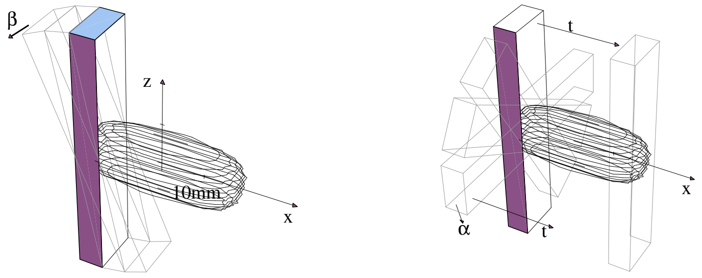

Fig. 8. Three-parameter sweep motion used for generating ellipsoidal high dose region with a static rectangular collimator. Beam is swept along translational direction t. This sweep is combined with rotational sweeps (parameters α, β).

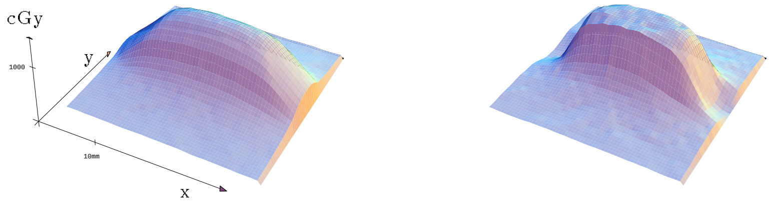

Fig. 9. 2-dimensional dose profile for ellipsoidal high dose region. a) Cylinder beam b) Rectangular beam. Height above x-y-plane represents dose. Much sharper focus of dose within ellipsoidal region is achievable with rectangular beam than with cylindrical beam.

3.1 Ellipsoidal Isodose Surfaces

A first series of experiments considers methods for generating non-spherical regions of high dose. An ellipsoidal shape is a very simple non-spherical shape. Figs. 9-12 compare two distributions with an ellipsoidal RHD. The first distribution was generated with a cylindrical collimator. The second distribution corresponds to a *static* rectangular collimator. The same motion was used in both cases. This motion is shown in fig. 8.

To evaluate the homogeneity of a distribution, one could consider the difference between maximum and minimum dose in the tumor region. However, this measure does not take into account the respective volumes of so-called hot spots and cold spots. A *dose-volume histogram* provides a more adequate way to evaluate homogeneity: for each percentage value x, the volume of tissue receiving $\geq x$ percent of dose is computed. The dose-volume histogram (DVH) shows the volume (ordinate values) absorbing dose $\geq x$ as a function of x (abscissa values). A DVH can equally be used to evaluate the distribution outside the tumor. An evaluation of the distributions for cylindrical/static rectangular collimators based on dose-volume histograms for lesion and surrounding tissue is shown in fig. 9-12. For each DVH, we compute the integral of the DVH-function and normalize to unit volume. The RHD is substantially more homogeneous for the rectangular collimator. In addition, the dose in the surrounding healthy tissue is lower for the rectangular collimator.

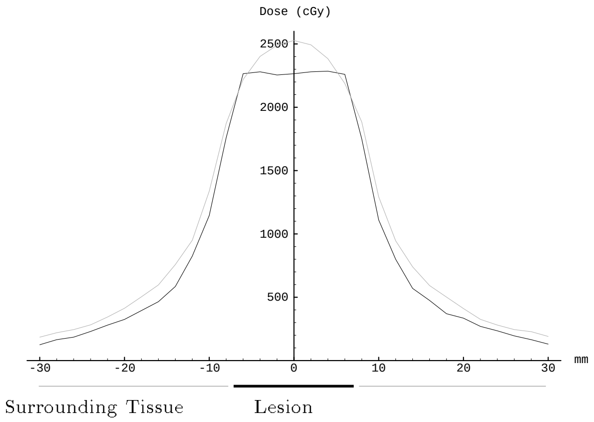

Fig. 10. 1-dimensional cross-sections of dose profiles (ellipsoidal high dose region). Gray curve: cylinder beam; black curve: static rectangular beam.

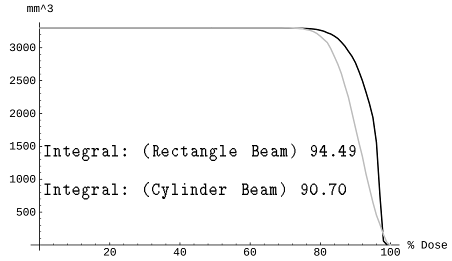

Fig. 11. Dose-volume histograms (lesion), ellipsoidal RHD. Black curve: rectangular beam; gray curve: cylinder beam.

3.2 Sample Case

Fig. 13-a shows a sample case with an arterio-vascular malformation (AVM). The malformation is delineated in the figures. The distribution generated with the described methods for a jaw collimator is shown in figs. 13-b through 15.

The dose distribution generated by a cylinder collimator (in the same case) using the planning methods in [10] was computed for comparison. Fig. 14 shows the dose-volume histograms for jaw and cylinder collimators respectively. In both cases, integrals were computed and normalized to unit volume. Substantially higher dose homogeneity is obtained for the adapatable collimator.

3.3 Non-convex shapes

The field partioning methods described in the previous section were evaluated in connection with manual and automatic beam weighting methods. Fig. 16 shows an example. The input to the planning system are the coordinates of cross-sections for the u-shaped region R (fig. 16-a). To generate a region of high dose matching this shape, a series of 600 rectangles in 40 planar projections were

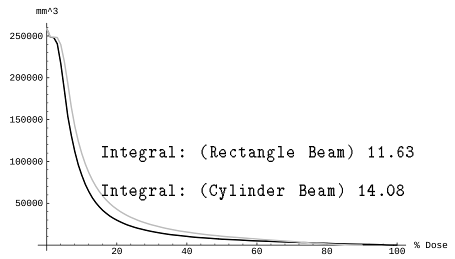

Fig. 12. Dose-volume histograms for ellipsoidal RHD (tissue surrounding lesion).

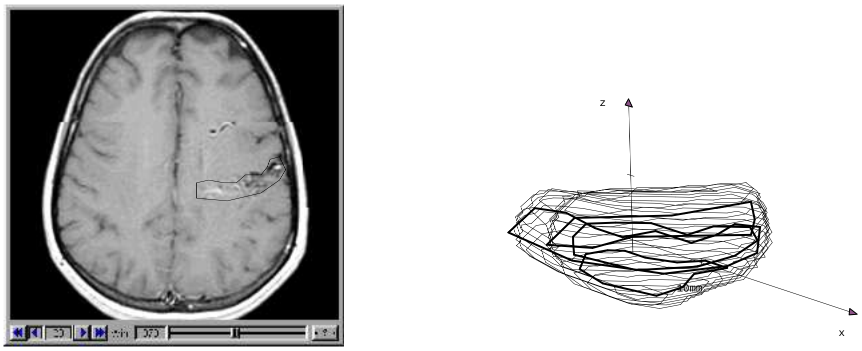

Fig. 13. a) Anatomy for sample case; arterio-vascular malformation (AVM) delineated. b) 80% isodose surface for distribution generated with adaptable jaw collimator (thin lines). Surface overlaid upon delineation of malformation. Bold lines: delineation of malformation in tomographic cross-planes.

overlaid. A constant rectangle width of 12 mm was used. The length of rectangles varies according to the projection shape. A critical region was delineated in the cavity of R. Automatic beam weighting based on arrangement computation was then applied to minimize weights of beams through the critical region while keeping the dose inside R between specified thresholds. Fig. 16-b shows the 80% isodosic surface generated in this way. Similar matching between input and output shape was unachievable with manual weighting.

4 Conclusions

We describe collimation methods for robotic radiosurgery. Paradigms for the interactive application of geometric algorithms are developed in this context. Geometric planning techniques have been combined with an algorithm for computing a path giving shortest total radiation time for a given maximum planar penumbra. The techniques include means for generating non-convex regions of high dose. Sweep methods for beam-shaping are particularly appropriate for robotic radiosurgery. Low cost, low collimator weight and high flexibility for generating complex distributions are the benefits of this approach.

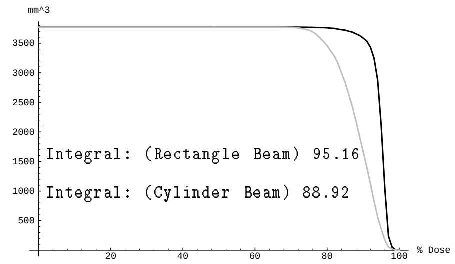

Fig. 14. Dose-volume histograms for the AVM in the sample case. Integral over histogram normalized to unit volume. Black curve: cylinder beam. Gray curve: rectangular beam

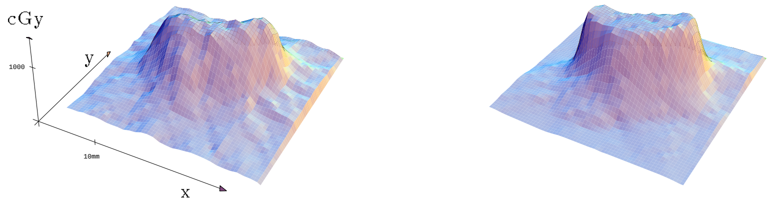

Fig. 15. Distribution cross-section for adaptable jaw collimator (AVM sample case). Height above x-y-plane represents dose. a) Cylinder beam. b) Rectangular beam.

A first series of experiments suggests that multiple-beam field shaping methods in connection with 6 degree-of-freedom beam motion can produce radiosurgical distributions with characteristics approaching the characteristics of spherical distributions.

References

1. Carol, M. An Automatic 3-D treatment planning and implementation system for optimized conformal therapy. Reprint of paper presented at 34th Annual Meeting Am. Soc. Therap. Radiology and Oncology, San Diego, Nov. 9-13, 1992.
2. Convery, D., Rosenbloom, M. The generation of intensity-modulated fields for

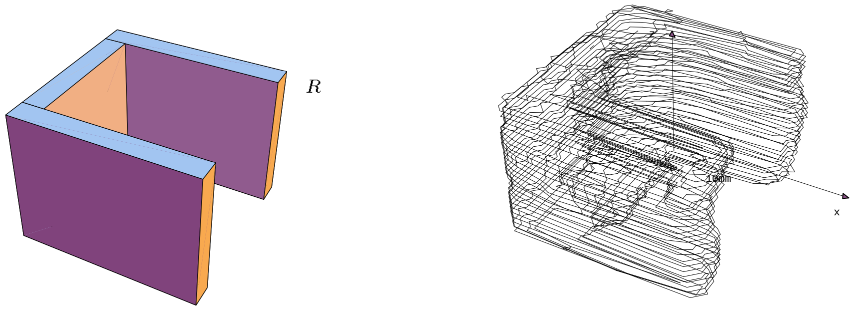

Fig. 16. a) Extruded u-shape. b) 80% isodose surface for distribution generated with jaw collimator and automatic beam weighting. RHD is an extruded u-shape

conformal radiotherapy by dynamic collimation. *Phys. Med. Biol.*, 36 (7): 1359–1374, 1992.

3. Kallman, P., Lind, A., Eklof, A., Brahme, A. Shaping of arbitrary dose distributions by dynamic multileaf collimation. *Phys. Med. Biol.*, 33 (11): 1291–1300, 1988.
4. Leavitt, D., Martin, M., Moeller, J. H., Lee, W. Dynamic wedge techniques through computer-controlled collimator motion and dose delivery. *Med. Phys.*, 17 (1): 87–91, 1990.
5. Lutz, W., Winston, K. R., and Maleki, N. A System for stereotactic radiosurgery with a linear accelerator. *Int. J. Radiation Oncology Biol. Phys.*, 14:373–381, 1988.
6. Podgorsak, E. B., et al. Dynamic Stereotactic Radiosurgery. *Intern. J. Radiation Oncology Biol. Phys.*, 14:115–126, 1988.
7. Nedzi, L. A., Kooy, H. M., Alexander, E., et. al. Dynamic Field Shaping for Stereotactic Radiosurgery: A Modeling Study. *Intern. J. Radiation Oncology Biol. Phys.*, 25:859–869, 1993.
8. Rice, R. K., et al. Measurements of Dose Distributions in Small Beams of 6 MeV X-Rays. *Phys. Med. Biol.*, 32:1087–1099, 1987.
9. Schweikard, A., Adler, J. R., and Latombe, J. C. Motion Planning in Stereotaxic Radiosurgery. *IEEE Tr. Robotics and Automation*, 9, 6, 764 - 774, 1993.
10. Schweikard, A., Bodduluri, M., Tombropoulos, R. Z., Adler, J. R. Planning, Calibration and Collision Avoidance for Image-Guided Radiosurgery. *Proc. IEEE Int. Workshop Intelligent Robots and Systems*, 854–861, 1994.
11. Starkschall, G., Eifel, P. An interactive beam-weight optimization tool for three-dimensional radiotherapy treatment planning. *Med. Phys.*, 19 (10): 155–164, 1992.
12. Webb, S. Optimization by simulated annealing of three-dimensional conformal treatment planning for radiation fields defined by a multi-leaf collimator. *Phys. Med. Biol.*, 36 (9):1201–1226, 1991.